Diurnal Changes in Cloud Cover in Eastern Gabon and Their Impacts on Energy Balance, Light Availability, and Water Demand: A Case Study of the 2022 Dry Season

Martin Magnan, Nathalie Philippon, Vincent Moron, Armand Mariscal, Olivier Liandrat

Diurnal changes in cloud cover in eastern Gabon and their impacts on energy balance, light availability and water demand: a case study of the 2022 dry season

Martin Magnan[a], Nathalie Philippon[a], Vincent Moron[b], Armand Mariscal[a], Olivier Liandrat[c].

[a] *Institut des Géosciences de l'Environnement, Université Grenoble Alpes, CNRS, IRD, Grenoble INP, Grenoble, France*

[b] *Aix-Marseille University, CNRS, IRD, INRAE, Collège de France CEREGE, Aix-en-Provence, France*

[c] *Reuniwatt, Toulouse, France*

Corresponding author: Martin Magnan, martin.magnan@univ-grenoble-alpes.fr

Early Online Release: This preliminary version has been accepted for publication in *Journal of Applied Meteorology and Climatology*, may be fully cited, and has been assigned DOI 10.1175/JAMC-D-23-0225.1. The final typeset copyedited article will replace the EOR at the above DOI when it is published.

ABSTRACT

Western Central Africa is atypical of the equatorial domain as the main dry season is cloudier than the rainy seasons. To understand this cloud cover's diurnal evolution, we set-up an infrared camera and acquired measurements of the total cloud cover fraction (TCF) and cloud optical depth at Bambidie, Gabon (0°44'30.5" S,12°58'12.4" O) from May to October 2022. Diurnal variations in TCF can be summarized into four types, mostly discretized through the timing and duration of clouds clearing in the afternoon (Early afternoon Clearing: EaC, Late afternoon Clearing: LaC and Clear Night: CNi) while one type (No Clearing: NoC) shows overcast conditions all day long.

Meteorological measurements show that NoC days record 50W/m^2 less shortwave incoming surface radiation resulting in daytime temperatures 1°C lower than the seasonal norm, but 20% more diffuse light and 0.5mm/day less ETo. Conversely, EaC days record 50W/m^2 more shortwave incoming surface radiation leading to temperatures 1.5°C higher than the seasonal norm, but 40% more direct light. The larger water demand (0.5mm/day more ETo) is partly compensated by more frequent rainfall at night-time.

The SAFNWC satellite estimates well capture the TCF variations for most of the 4 types. They confirm that TCF is dominated by very low and low clouds whose dissipation in the afternoon and evolution into fractional and cumuliform convective clouds explains the clearings on EaC and LaC days. Satellite estimates also show that the 4 types of days extracted at Bambidie are representative of a larger-scale cloud cover evolution in Western Central Africa, with a W-E gradient in the timing of afternoon cloud dissipation.

Accepted for publication in *Journal of Applied Meteorology and Climatology*. DOI 10.1175/JAMC-D-23-0225.1.

1. Introduction

Low-level clouds are key components of the weather and climate in many regions but are usually not well represented in atmospheric models (Nam et al. 2012). Recently, it has been shown that an extensive low-level cloud cover, mainly made up of stratiform clouds, develops during the June-September (JJAS hereafter) main dry season in western Central Africa (i.e., Southern Cameroon, Equatorial Guinea, Gabon and the Republic of Congo), with on average, the low-level clouds representing 70% of the total cloud cover (Dommo et al. 2018; Champagne et al. 2023). The combination of a rather long dry season with an opaque and long-lasting stratiform cloud cover is unique across most of the tropical land masses where the dry season is much less cloudy than the rainy season, as over the rest of Central Africa, the Amazon and South-East Asia.

This cloudy dry season in Western Central Africa (WCA hereafter) – which is also the longest (4 months) and driest (< 1mm/day in mean) relatively to other equatorial sectors – likely explains the presence of the densest evergreen forests (Réjou-Méchain et al. 2021), despite a relatively small total amount of rainfall relatively to the Amazonian basin and the Maritime Continent. This anomaly is mostly due to the low-level cloud that ensures relatively cool, humid and light-deficient atmospheric conditions (Philippon et al. 2019). A significant reduction of this cloud cover due to climate change may represent a major tipping point for WCA forests. Such change may be potentially threatening here since the rate of deforestation and degradation remains low (Duveiller et al. 2008). This would also negatively impact on the ecosystem services provided by these forests, including sources of moisture for the neighboring drier regions (Spracklen et al. 2012) and a huge carbon sink (Hubau et al. 2020). So far, the existing studies on WCA climate are few - the contemporaneous climate of Central Africa remains one of the most under-studied because ground-based observations are scarce - and have concentrated on the rainy seasons. Therefore, there is an urgent need to better understand the presence, variability as well as the bioclimatic effects of the low-level cloud cover in WCA.

Recent studies, conducted as part of the “Dynamics, variability and bioclimatic effects of low clouds in western central Africa” (DYVALOCCA) project, and mostly based on ground observations from trained observers (Aellig et al. 2022; Moron et al. 2023) and satellite imagery (Champagne et al. 2023), focused on this stratiform cloud cover to better understand its mean spatial distribution and diurnal evolution. The stratiform cloud cover is not spatially

Accepted for publication in *Journal of Applied Meteorology and Climatology*. DOI 10.1175/JAMC-D-23-0225.1.

homogeneous over the whole WCA: the cloud deck is thicker and more permanent over the coastal plains and windward slopes of the main mountain ranges of Gabon (Chaillu and Cristal mounts, cf. Figure 1) and southwestern Republic of Congo, than over the leeward slopes and the inner plateaux. The typical diurnal evolution of the cloud cover consists of afternoon clearings and a resettlement during the early night with low cloud fraction usually peaking from late night to noon (Moron et al. 2023), but about a third of the days shows an almost overcast sky all day long.

In WCA however, ground observations of the cloud cover from trained observers remain too scarce to fully picture and understand the diurnal cycle of the cloud cover: although supposed to be at 3-hourly resolution, there are far fewer ground observations during the night and also less on the eastern part of WCA where the network of weather stations is coarser. In addition, and so far, the impact of this low-level cloud cover on the energy budget, the light available for trees photosynthesis, and the water demand, despite important for forests functioning, has not been evaluated for WCA, as appropriate in-situ measurements were not available. For instance, diffuse light has been shown to increase primary productivity at the ecosystem and leaf level (Mercado et al. 2009; Berry and Goldsmith 2020). Satellite retrievals are ordinarily used to fill in the lack of ground observations, but they have their own shortcomings. A major difficulty stands in detecting low-level clouds at night especially in the tropics: as the low-level clouds top temperature is then close to the ground one, satellites often falsely detect a cloud free land. The use of night-time microphysical schemes partly reduces biases in the night-time detection of low clouds (Champagne et al. 2023). Another issue occurs around sunset and sunrise when the solar zenithal angle is low and the channels used for cloud detection change, leading to high uncertainties in the estimation of the presence of low-level clouds (Jedlovec et al. 2008; Derrien and Le Gléau 2010). Lastly, in case of a multi-layered cloud cover, the low-level clouds are also difficult to detect by satellites. However, as shown by Dommo et al (2018) such cases are infrequent in WCA and JJAS.

The use of infrared (IR) cameras can partly overcome the lack of ground observations of the cloud cover by trained observers especially at night-time, as well as the satellites biases, as they provide images at very high temporal resolution (usually <1min) along the whole diurnal cycle. For example, such cameras were used jointly with high resolution measurements from ceilometers, wind-profilers, and scanning microwave radiometers to accurately assess the times of formation and dissipation of the low-clouds cover in Southern West Africa and understand

Accepted for publication in *Journal of Applied Meteorology and Climatology*. DOI 10.1175/JAMC-D-23-0225.1.

the underlying physical processes (Dione et al. 2019; Lohou et al. 2020). Coupled with visible cameras during daytime, they can be used to deduce cloud type and characteristics (Wang et al. 2021) especially to forecast short term power photovoltaic production.

In 2022, we had the opportunity to set-up an IR camera for 6 months at Bambidie (0°44'30.5" S,12°58'12.4" O, 300 m asl), a city located in eastern Gabon, in the vicinity of the Oogoué valley (Figure 1). The IR camera was installed within the Precious Woods logging company's plot, next to a high-quality weather station that operated from March 2020 to March 2023, with the objective to improve our understanding of diurnal changes in the cloud cover in the dry season and assess its impact on key climate parameters for rainforests functioning.

By jointly analyzing high temporal resolution records of (i) the total cloud cover fraction (TCF hereafter) acquired with the IR camera, (ii) meteorological parameters (e.g. incoming, outgoing, diffuse radiation, etc.), acquired with the weather station, as well as satellite estimates of the cloud cover (e.g. TCF, cloud top height), we are seeking to answer the following questions:

1- What is the agreement between the diurnal changes of the cloud cover observed with an IR camera at a single station during a single season and those analyzed by Champagne et al. (2023) and Moron et al (2023) using satellite and ground observations from trained observers at larger spatial scales but also with a lower time resolution than here? Specifically, what new knowledge do we gain about the timing of amplitude and type changes in the cloud cover, particularly at night-time, when the ground observations are far less numerous, and the satellites are less accurate to detect low cloud cover than during daytime?

2- What changes in the diurnal evolution of incoming and outgoing surface radiation, of the quantity and quality of light available for photosynthesis by trees, are driven by the cloud diurnal variations? How does the water demand vary under the different cloud covers?

3- To what extent are the local observations made at Bambidie representative of the diurnal evolutions of the cloud cover over a larger area of WCA?

To that aim, typical diurnal evolutions of the local TCF (referred to as "canonical types") are defined as in Moron et al. (2023). These canonical types are then systematically compared with (i) the diurnal evolutions of meteorological parameters recorded at the weather station to assess the corresponding modulations, in sign and amplitude, of the radiative budget, light availability

Accepted for publication in *Journal of Applied Meteorology and Climatology*. DOI 10.1175/JAMC-D-23-0225.1.

and water demand, and with (ii) satellite estimates of the cloud cover enabling the analysis of changes in the clouds in presence as well as the identification of spatial patterns and scale of the low cloud cover across WCA.

The paper is organized as follows: section 2 describes the different datasets used in this study, namely the IR camera images, the weather station measurements and the satellite cloud products; details on the methodology used especially to extract the canonical types and to assess the significance of the results are also depicted in this section. Section 3 presents first a quick overview of the 2022 dry season, at Bambidie (Sect. 3.a), then the canonical types of the TCF diurnal evolutions (Sect. 3.b) and the respective modulations observed in the energy budget, light availability, and water demand (Sect. 3.c). The cross-analyses with satellite cloud products are presented in Sect. 3.d. At last, the main results are discussed in Sect. 4, followed by the conclusions.

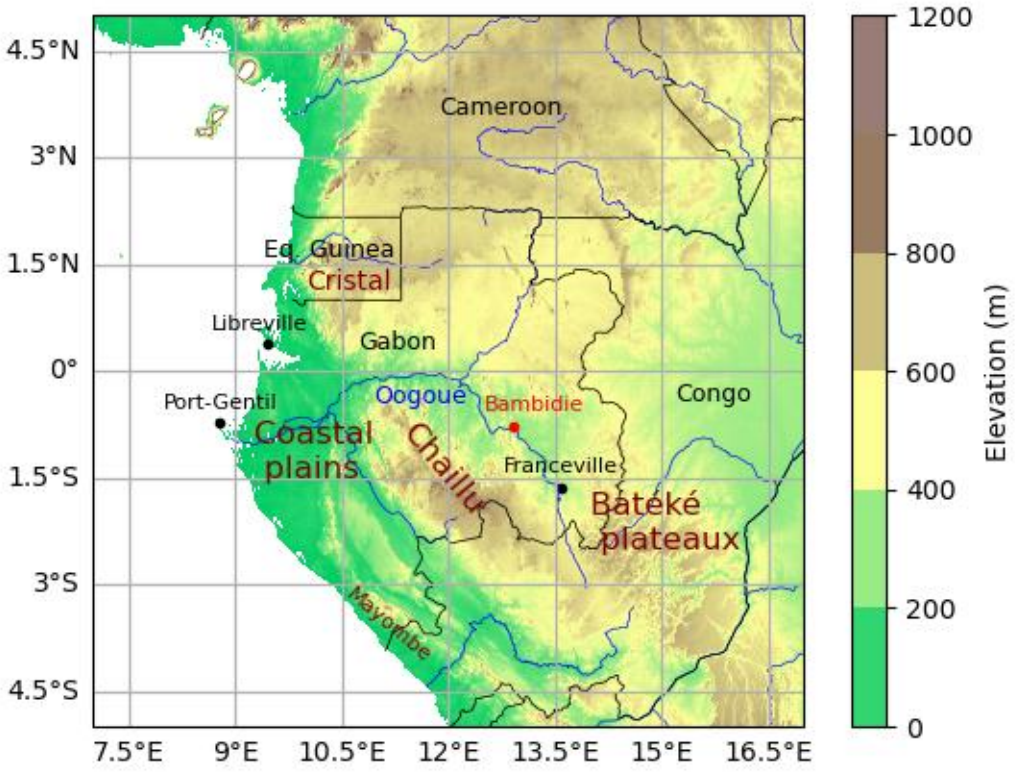

Figure 1: Geography and topography (in meters) of the study area

2 Data and methods

a. The Sky-Insight Infra-Red Camera from Reuniwatt

Accepted for publication in *Journal of Applied Meteorology and Climatology*. DOI 10.1175/JAMC-D-23-0225.1.

The Sky InSightTM is a sky imager composed of a thermal-infrared camera (8-14μm) aiming downward at a chrome-coated hemispheric mirror, which allows it to provide sky images with a field of view of 180° and a temporal frequency of 30 seconds. An algorithm developed by Reuniwatt is used to determine whether a pixel is cloudy or not based on the IR camera, radiance, temperature and humidity sensors (Bertin et al. 2015; Liandrat et al. 2017). The TCF is then calculated counting the number of cloudy pixels over the total number of pixels with a limitation on the zenith angle of 80°. Figure S1 gives an example of the brightness temperature of the sky (left), and the cloud mask and cloud fraction (right) deduced from the former for the 13th of July 2022 at 12.00 UTC / 13.00 LST. The Cloud Optical Depth (COD) is also considered in this study as both variables (TCF and COD) affect the incoming surface radiation. The COD estimation from the Sky InSight is based on a proprietary Reuniwatt algorithm. The basics of the algorithm are described in Bertin et al. 2015. First, clear-sky radiance is estimated from humidity and temperature measurements and a priori knowledge of the site based on ECMWF climatologies and LibradTran simulations. The clear sky radiance is subtracted from the overall radiance perceived by the camera to retain only the cloud contribution. Finally, a linear relationship is applied to the residual radiance to estimate the COD for every pixel of the images (Bertin et al. 2015).

Given the zenith angle, the spatial sky coverage radius can be calculated using the formula $R = H*\tan(80°)$ knowing the cloud ceiling (H). With a cloud ceiling set at ~1 km above ground level (as is generally observed over WCA in JJAS due to the extensive low cloud cover that develops, Dommo et al 2018) the radius would be 5.7 km, and the camera would cover a sky area around 100 km².

To be sure to fully capture the whole dry season, the Sky InSightTM camera was installed at Bambidie, a few meters apart from a high-quality weather station, from May 8 to October 17, 2022, thus for 162 days. However, as in many in-situ measurement systems, the camera encountered technical problems such that some 30-sec time steps are not documented (Figure S2 bottom) and only 99 of the 162 days of the field campaign had no missing data.

b. The weather station

A Campbell weather station was installed from the 6th of March 2020 to the 16th of March 2023 at Bambidie. In addition to the usual meteorological parameters (i.e., temperature, humidity, precipitation, wind speed and direction, sea level pressure), measured every 15 min, more specific parameters related to irradiance (i.e., short and long wave incoming and

Accepted for publication in *Journal of Applied Meteorology and Climatology.* DOI 10.1175/JAMC-D-23-0225.1.

outgoing, global and diffuse, and Photosynthetic Active radiations) and soil temperature and moisture (at 10, 20, 50 and 100 cm depth), were also measured every minute. Table S1 in supplementary materials lists the sensors and parameters used for the present study and which were cross-analyzed with the TCF and COD data issued from the IR camera, while Figure S2 (top) shows that very little data was missing during the 2022 dry season.

c. Satellite cloud properties from SAFNWC

To fully understand the cloud cover evolution at Bambidie and how it fits into a wider spatial scale, Cloud Type (CTYPE hereafter), Cloud Top Temperature and Height products from SAFNWC (NoWcasting and very short-range foreCasting Satellite Application Facilities), generated by the Service d'Archivage et de Traitement Météorologique des Observations Satellitaires were used for this study. Those products are calculated from Meteosat Second Generation satellite imagery with a 3-km spatial resolution and 15-min temporal resolution from 2008 to date which allows us to further document the diurnal cycle of cloudiness at Bambidie from 1st May - 31st October 2022 and over the whole WCA.

The CTYPE product classifies pixels into 15 different classes on the basis of algorithms using bidirectional reflectances and brightness temperatures of 10 channels from the Spinning Enhanced Visible and Infrared Imager on-board Meteosat Second Generation, combined with numerical weather prediction, climatological fields of temperature (from surface to tropopause level) and total water vapor content (Derrien and Le Gléau 2005, 2010); for a full documentation of the algorithm see http://www.nwcsaf.org/ web/guest/scientific-documentation.

Amongst the 15 classes available, the “sea ice” and “snow over land” ones do not occur in WCA. 5 classes are dedicated to the high semi-transparent clouds which were grouped into a single class. Similarly, we grouped into a single class the high and very high opaque clouds. Therefore, the resulting 7 classes are: cloud free land, very low clouds (below 2000m above sea level), low clouds (2000-3500m), mid-level clouds (3500-6500m), opaque clouds, high semi-transparent clouds (both above 6500m) and fractional clouds.

The Cloud Top Temperature and Height product provides the cloud top temperature (in Kelvin) and altitude (in meter). Both are derived from IR brightness temperatures from 7 channels (from 6.2 to 12.0 μm) by comparison to simulated IR brightness temperatures computed from temperature and humidity vertical profiles from numerical weather predictions

Accepted for publication in *Journal of Applied Meteorology and Climatology.* DOI 10.1175/JAMC-D-23-0225.1.

using an IR radiative transfer model. Note that the CTYPE serves as input in the computation process of the cloud top height (CTH hereafter): indeed, they are also derived from the cloud top pressure retrieval methods which depend on the CTYPE.

In presence of an extensive low cloud cover as it is the case in JJAS in WCA, and according to ground observations by trained observers (Dommo et al. 2018), an approximation is made, considering the cloud base height to be around 1 km above the ground. Therefore, as discussed in section 2.1, such height represents an approximate area of 100 km² sky coverage for the IR camera. As the SAFNWC cloud products spatial resolution is 3 km, a 3 by 3 pixel window (81 km²) is therefore needed to cover approximately the same area as the IR camera. The satellite TCF that is used hereafter is calculated from the CTYPE product using a 3 by 3 pixel window centered on Bambidie. Ten different values are then possible ranging from 0 (none of the nine pixels are cloudy) to 1 (the nine pixels are cloudy).

d. K-Means algorithm, significativity tests, deseasonalization and standardization procedure

First, the K-Means algorithm is designed to separate *n* observations in *k* groups, called "clusters". Each cluster is described by the mean μ of the observations assigned to it and called the cluster "centroid". The K-means algorithm aims to find centroids that minimize the inertia, or within-cluster sum-of-squares.

$$\sum_{i=0}^{n} \min_{\mu_j \in C} (\|x_i - \mu_j\|^2)$$

The K-means method was used to cluster the 162 available days according to the diurnal evolution of the TCF. Each day (or observation) is composed of 2880 TCF values i.e., one per 30 seconds. The classification was made on the 99 days without missing data. The 55 days with a few missing data were classified using the minimal Euclidean distance from the centroids computed from the 99 complete days. The 8 days with an excessive amount of missing data were discarded (gray patches in the calendar plot in Figure 3c). In total, 154 days are clustered.

Second, to assess the significance of the results (e.g. the differences observed in the different meteorological parameters between the 4 canonical types), random draws were performed for different analyzes of the study (Figures 4, 5, 7, 10 and S4) to generate new distributions with which to test our results. The size of each draw equals the number of days of the canonical type tested. The number of draws (with replacement) ranged from 500 to 2000 (depending on the parameter analyzed). Then the percentiles 2.5th and 97.5th were calculated

Accepted for publication in *Journal of Applied Meteorology and Climatology*. DOI 10.1175/JAMC-D-23-0225.1.

from those distributions. The comparison between the percentiles and our results allowed us to assess if they are distinct from randomness, with a 95% level of confidence. For instance, Figure 4 shows the comparison between the diurnal TCF evolution for the 4 canonical types and the corresponding 2.5th and 97.5th envelope obtained from the random draws.

Third, to provide a fair comparison of the canonical types whose occurrence along the seasonal cycle is not identical, we deseasonalized all the variables analyzed. The day of year means from the 3 available seasons were subtracted from the daily values for the 2022 season, resulting in deseasonalized daily anomalies.

Last, to perform a diurnal cycle of the evolution of CTH and compare the 4 canonical types, values were standardized with respect to their CTYPE. For each CTYPE, mean and standard deviation were calculated over all the timestamps. CTH standardized values were then obtained by subtracting the mean and dividing by the standard deviation.

e. Evapotranspiration calculation

The hourly evapotranspiration was calculated using the Penman-Monteith equation given below using measurements from the weather station (Table 1). ETo was deseasonalized in Figure 6 to compare the four canonical types which are not distributed equally along the measurement period.

$$ET_o = \frac{0.408\Delta(R_n - G) + \gamma \frac{37}{T_{hr} + 273} u_2 (e^o(T_{hr}) - e_a)}{\Delta + \gamma(1 + 0.34u_2)}$$

where

ETo: reference evapotranspiration [mm.hour^{-1}],

R_n: net radiation at the crop surface [MJ.m^{-2}.hour^{-1}],

G: soil heat flux density [MJ.m^{-2}.hour^{-1}],

T: air temperature at 2 m height [°C],

u_2: wind speed at 2 m height [m.s^{-1}],

$e^o(T_{hr})$: saturation vapor pressure [kPa],

e_a: actual vapor pressure [kPa],

Δ: slope vapor pressure curve [kPa.°C^{-1}],

Accepted for publication in *Journal of Applied Meteorology and Climatology*. DOI 10.1175/JAMC-D-23-0225.1.

γ: psychrometric constant [kPa.°C^{-1}].

Some parameters are measured (R_n, u_2, T), others are calculated (G, $e^o(T_{hr})$, e_a, Δ, γ, P) using measured parameters (RH, P, T) with the formulas below:

G_{hr} = 0.1 R_n during daylight and G_{hr} = 0.5 R_n during nighttime

$$e^o(T_{hr}) = 0.6108 \exp\left(\frac{17.27T_{hr}}{T_{hr} + 237.3}\right)$$

$e_a = e^o(T_{hr}) \frac{RH_{hr}}{100}$ where RH_{hr} is the average hourly relative humidity (%)

$$\Delta = \frac{4098\left[0.6108 \exp\left(\frac{17.27T_{hr}}{T_{hr} + 237.3}\right)\right]}{(T_{hr} + 237.3)^2}$$

$\gamma = 0.665 * 10^{-3} P$ where P is the atmospheric pressure (kPa).

3. Results

a. The daily cloudiness and meteorological conditions during the 2022 dry season

Figure 2a shows the evolution from May to October 2022 of the daily TCF, rainfall, ETo and soil wetness at 20 cm recorded at Bambidie (with TCF and ETo values filtered with a 7-day running mean). The 2022 dry season is clearly identified without almost any precipitation from mid-June to mid-September and a concomitant soil wetness decrease (from 0.4 to 0.3 m^3/m^3). Despite the onset of the dry season in mid-June, changes in TCF are subtle: levels are generally above 60% for most days during the dry season, and the TCF mean for the analyzed period is around 74% for both IR Camera and satellite. However, TCF levels from the camera are slightly higher for the period from mid-June to mid-August while ETo levels are the lowest at the same time. The dry season in WCA is typically associated with stratiform non-precipitating clouds (Philippon et al. 2019; Dommo et al. 2018; Champagne et al. 2023). Although from TCF alone it is not possible to distinguish stratiform from convective clouds. Most of the days are not rainy (111 days without rainfall out of the 162 days of the camera's measurements) and most of the rainy days recorded a low rainfall amount (less than 5 mm for 36 out of 51 days) which is characteristic of a stratiform low cloud cover. Lastly, it should be noted that the 2022 dry season seems to be rather normal in terms of timing and anomalies of the low cloud fraction and rainfall vs the last 30 years (Figure S3). We thus believe that it provides a good example of typical diurnal variations of the dry season cloud cover over WCA.

Accepted for publication in *Journal of Applied Meteorology and Climatology*. DOI 10.1175/JAMC-D-23-0225.1.

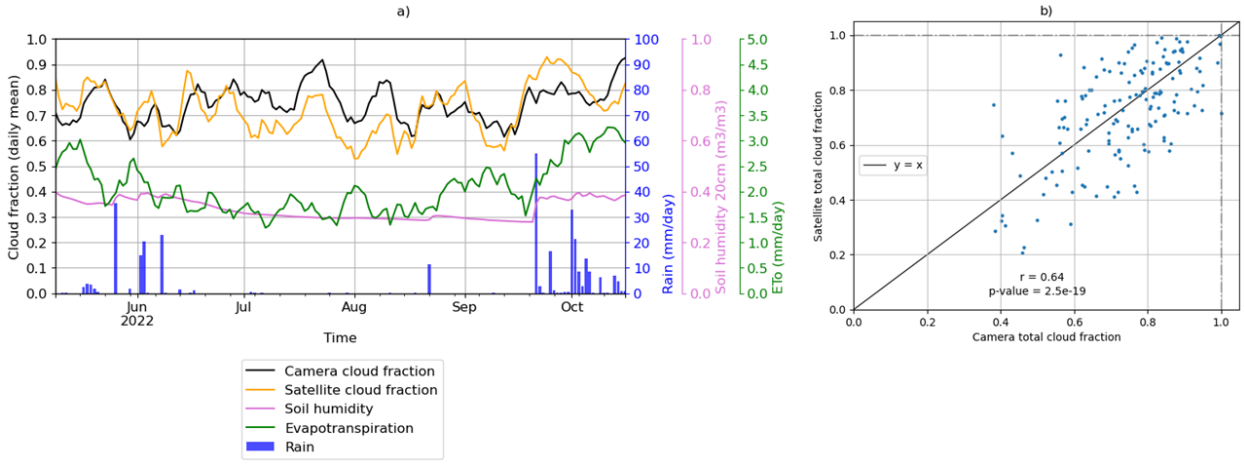

Figure 2: a) 7-day rolling means of ETo (green, estimated from the weather station measurements) and TCF (black, as measured by the IR Camera, days with less than 75% of available data are discarded) and estimated from SAFNWC (yellow) at Bambidie from the 8th of May to the 17th of October 2022. The daily rainfall accumulations are also depicted as blue bars and the daily soil wetness at 20cm as the purple line. b) Scatterplot of the IR camera vs SAFNWC daily means of the TCF (r = 0.64, significant at 95%).

b. The canonical diurnal types of TCF

In their study focused on the low-level cloud cover only, Moron et al (2023) and Champagne et al (2023) showed that it was characterized by specific diurnal evolutions. They extracted three "canonical types": days totally overcasted by low-level clouds, days with an afternoon clearing of the low-level cloud cover and days with a low cloud cover.

The diurnal evolutions of the TCF at Bambidie during the 2022 dry season are explored below and the questions we are seeking to answer are: how does the TCF evolve during the diurnal cycle at Bambidie? What are the average times at which clouds settle and dissipate? To what extent are the evolutions observed at Bambidie in agreement with the canonical types extracted by Moron et al (2023)? What are the changes during the dry season in relation to the seasonal cycle?

Figure 3a shows the TCF diurnal evolution of the 4 canonical types (or centroids, colored lines) retained with respect to the mean of all days (gray bars). The x-axis represents the local time (UTC +1) and hereafter every mention of time will refer to this time zone. Figure 4 shows the TCF diurnal evolution (with the respective +/- 0.5 std envelope) of the four types, as well as the envelope with respect to the 2.5 and 97.5 percentiles obtained from the random draws (gray envelope, cf. section 2.5). Whatever the canonical type, the two envelopes overlap mostly during late night and morning which is fully consistent with the fact that the temporal spread

Accepted for publication in *Journal of Applied Meteorology and Climatology*. DOI 10.1175/JAMC-D-23-0225.1.

is then minimal: basically, TCF is then almost always very high (Figure 3) and any random selection of days leads to similar (high) means as those of any of the types (Figure 4). So, types are mostly distinguished by the TCF evolution from 12.00 to 04.00 (Figure 3). This result matches well with what is observed over a larger sample of stations, covering Gabon and SW of the Republic of Congo, and numerous dry seasons (Champagne et al. 2023; Moron et al. 2023), i.e., most of the diurnal variance of the cloud cover is determined by the clearings of the stratiform clouds during the afternoons and early evenings, while the nighttime and morning cloudiness is more compact and less variable.

Out of the four types, three have clearings in the afternoon (Figure 3). The only type with no clearing at all, the "no clearing" one (NoC hereafter), is the most frequent (37.7% of the total number of days). For this type, the TCF remains high (above 0.8) almost the whole day. On the contrary, the "clear night" type ("CNi", 13%) has by far the lowest daily mean TCF of the 4 types. It is characterized by a clearing from 13.00 to 19.00 (with TCF values significantly lower than randomness from 15.00 until 03.00, Figure 4).

The "early afternoon clearing" ("EaC") and the "late afternoon clearing" ("LaC") types display very similar daily mean TCF (respectively 0.77 and 0.69). However, both types differ in the clearing timing. The LaC type (31.2%) displays a clearing from 13.00 until 19.00 (with TCF significantly lower from 17.00 to 22.00, Figure 4). While the EaC type (18.2%) displays a clearing, from 11.00 to 16.00 (TCF significantly lower than the randomness from 12.00 to 17.00, Figure 4). This type possesses the highest nighttime TCF.

The frequency of occurrence of the four types along the dry season (Figure 3b and c) shows a prevalence of the NoC days during the heart of the dry season (more than 45% of the days in July-August) as also observed by Moron et al. (2023) using a large dataset of low-level clouds observations. Note that the CNi and the EaC days are more frequent at the beginning and at the end of the dry season with more than 75% of the EaC days in the month of May, September and October. This is also in agreement with findings by Moron et al (2023).

For each canonical type, the corresponding COD diurnal evolution is presented in Figure 5b. It is noteworthy that COD diurnal evolutions are very close to the TCF ones for most of the types (COD/TCF correlations are >0.9 for NoC, CNi and LaC days, against 0.76 for EaC). This agrees with the fact that the stratiform low-level clouds dominate, and suggests that their breaking-up in the afternoon is accompanied with their thinning. The least match between TCF and COD on EaC days is noticeably due to a ~2-h lag between the TCF and COD minima,

Accepted for publication in *Journal of Applied Meteorology and Climatology*. DOI 10.1175/JAMC-D-23-0225.1.

suggesting a transition towards more cumuliform low-level clouds (confirmed in section 4 with satellite cloud products) with higher COD.

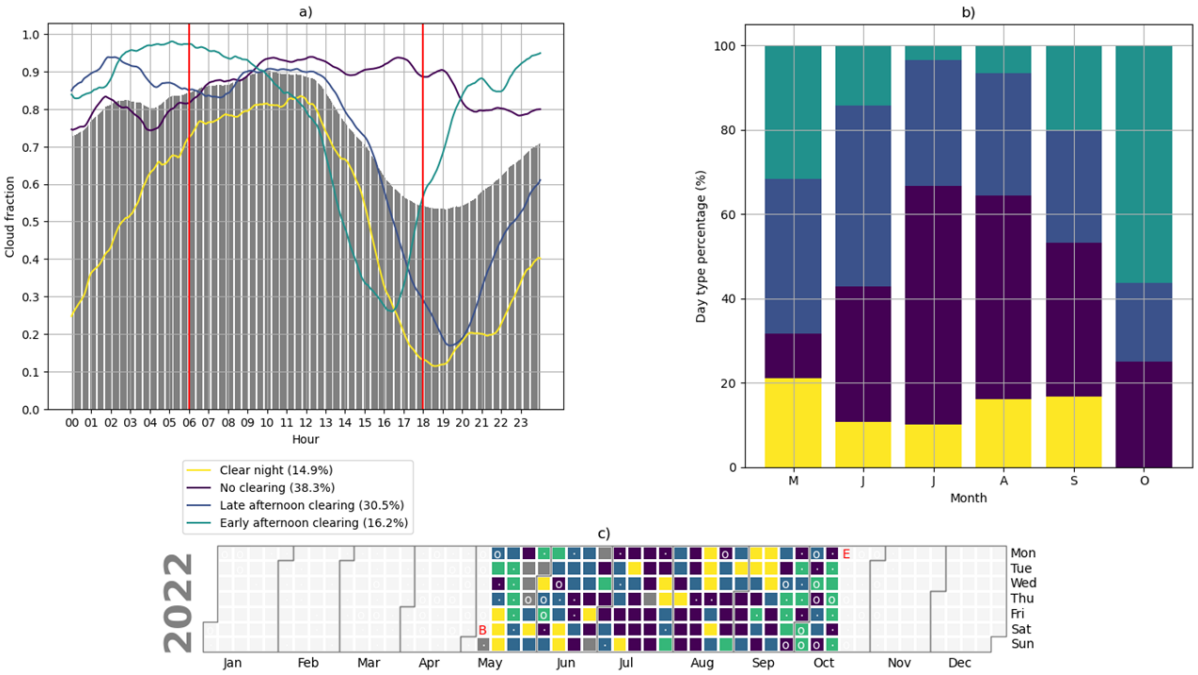

Figure 3: (a) The 4 "canonical types" of TCF at Bambidie extracted with a K-Means classification (gray bars: mean TCF, colors: mean TCF of each type, red lines: sunrise and sunset, filtered with a 1-hour rolling mean) with the local time on x-axis. (b) The frequency of occurrence by month of each type during the 2022 dry season (the months of May and October are incomplete). (c) the corresponding calendar plot; B and E mark the beginning and end of the field campaign; the 8 discarded days are in gray. White dots (circles) represent rainy days with amounts between 0.1 and 5mm (>5mm).

Accepted for publication in *Journal of Applied Meteorology and Climatology*. DOI 10.1175/JAMC-D-23-0225.1.

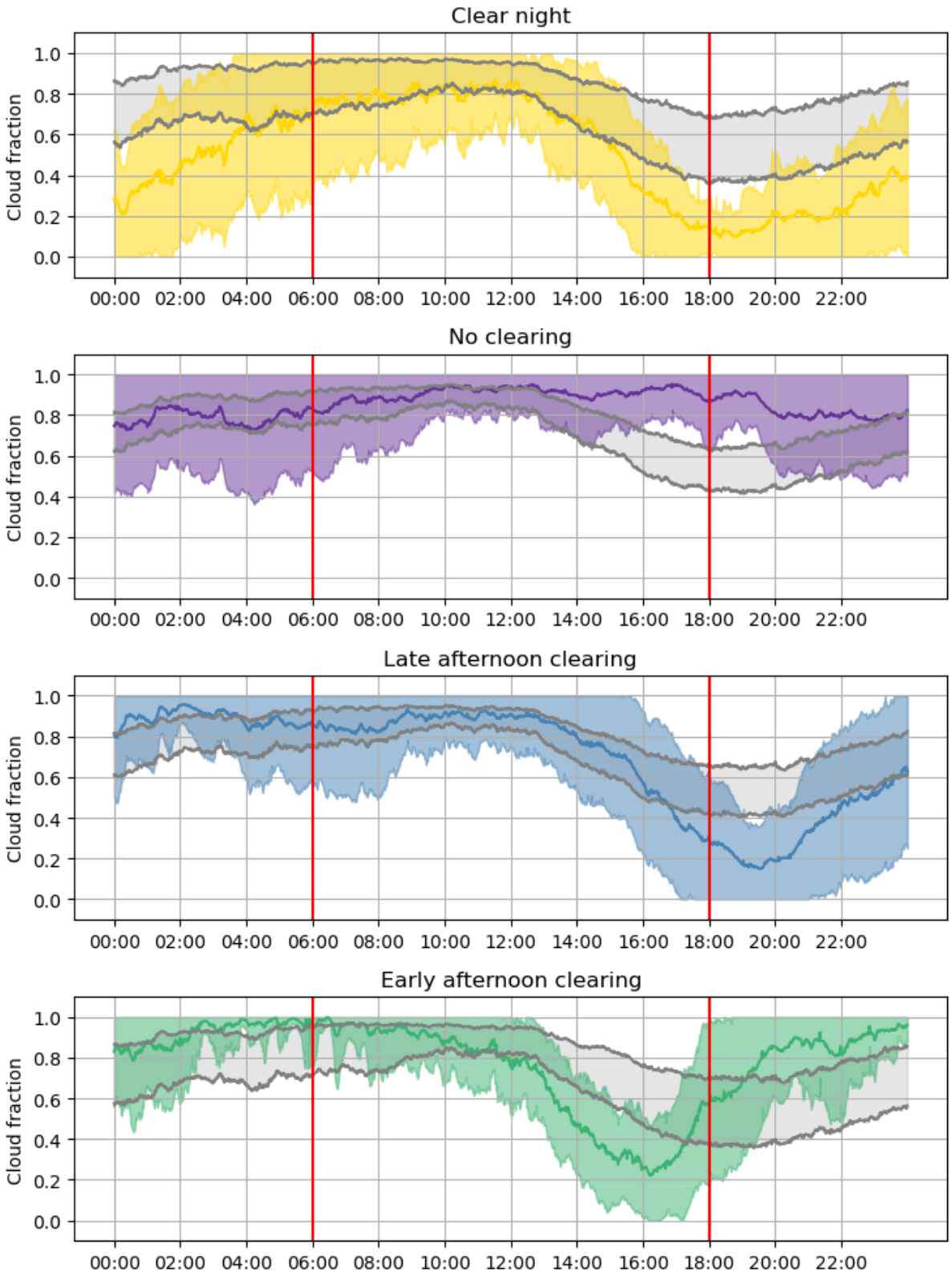

Figure 4: The mean TCF for the 4 canonical types (colored line) with the respective +/- 0.5 std envelope as colored area. Gray areas correspond to the range between the 2.5th and the 97.5th quantiles obtained from 500 random draws (with replacement) of TCF for each type (each draw is composed of the same number of days as the chosen type). Red lines: sunrise and sunset. X axis: local time.

Accepted for publication in *Journal of Applied Meteorology and Climatology*. DOI 10.1175/JAMC-D-23-0225.1.

c. TCF impact on energy budgets, water demand and light availability

The question that now arises from the results of the classification is as follows: what are the modulations observed in the quantity and quality of light available for trees photosynthesis, and water demand and availability under these different evolutions of the total cloud cover? Do the different diurnal evolutions of the cloud cover result in significantly different levels of incoming, outgoing, diffuse and Photosynthetically Active (PAR) surface radiations, evaporation, and rainfall?

The classification performed allows a broader analysis of the impacts of TCF variations at the diurnal timescale on the meteorological parameters that are measured at Bambidie. The goal is to understand the modulation of radiation at the surface and water demand.

For each canonical type, the clearness index (KC), the rainfall frequency of occurrence, the 2-m air temperature, the net and incoming longwave surface radiation (LWnet, LWin), the incoming shortwave surface radiation (SWin), the photosynthetically active radiation at the surface (PAR), the direct/diffuse surface radiation ratio anomalies are calculated along the diurnal cycle and plotted in Figure 5. It should be noted that the net total, and LWout surface radiations on the one hand, and the net SW surface radiation on the other, have diurnal behaviors close to the 2-m air temperature, and the SWin respectively, and are therefore not displayed. All the radiation is measured at ground level, and therefore any further mentions of radiation should be considered as surface radiation. The clearness index KC is a ratio between the irradiance recorded on the ground and the Clear Sky Irradiance. That latter is the maximum irradiance, i.e., the irradiance in perfect clear sky conditions which depends only on the latitude and day (without disturbance between the top of the atmosphere and the ground).

1) THE ENERGY BUDGETS

Among the 4 types, LaC is the one associated with the weakest anomalies for most of the parameters, anomalies that are most of the time not significant. This means that this type of day is the most typical/representative of the dry season. The only significant signal observed is a deficit in the incoming longwave radiation (LWin, Figure 5f) between 17.00 and 21.00 in response to the peak of the clearing and the COD minima (Figures 3a and 5b) and which translates into the net radiation (LWnet, Figure 5f-i). A direct consequence is the lowering of the temperatures by about -1°C from 20.00 to 22.00 (Figure 5h).

Accepted for publication in *Journal of Applied Meteorology and Climatology*. DOI 10.1175/JAMC-D-23-0225.1.

On CNi days, KC anomalies (Figure 5c) keep increasing throughout the day as the sky clears progressively during daytime (Figure 3a). At night, the lower cloud cover produces anomalies of around -10W/m2 for LWin (Figure 5f) and -1.5°C for temperature (Figure 5h). During the day, incoming shortwave radiation anomalies are always significantly positive (+50W/m2 on average, Figure 5e), the highest in the early morning as the cloud cover is not fully resettled which induces temperatures 0.8°C higher than normal (and LWout anomalies above 10W/m2, not shown). As a result, net longwave radiation anomalies (Figure 5i) are always significantly negative (-10W/m2 on average), and the lowest of the 4 types.

The EaC days are similar to the CNi days in some aspects. KC is the highest of the four types: it keeps increasing along the day confirming that the sky is becoming clearer and clearer (with positive anomalies being significant from 10.00 to 16.00). Incoming longwave radiation displays significant positive anomalies (+5W/m2) around sunrise, when the TCF is the highest, and after sunset (Figure 5f). During daytime, the clearer sky leads to incoming shortwave radiation 50W/m2 higher than normal. This surplus of radiation induces warmer temperatures than in the other types of days, up to 1.5°C higher than normal in the afternoon.

On NoC days, KC anomalies decrease all day long indicating that the sky is getting cloudier than in the other classes (Figure 5c). Net longwave radiation anomalies are mostly positive (higher than 8W/m2 from 11.00 to 20.00, Figure 5i), in response to a significant surplus of incoming radiation around sunset (+5W/m2) consistent with the large cloud fraction then, and a significant deficit of outgoing radiation during the day (up to -10W/m2 not shown). On the other hand, incoming shortwave registers a deficit of -50W/m2 on average, so these days are the coolest during daytime with temperatures more than 1°C below normal from 13.00 to 18.00 (Figure 5h).

Accepted for publication in *Journal of Applied Meteorology and Climatology.* DOI 10.1175/JAMC-D-23-0225.1.

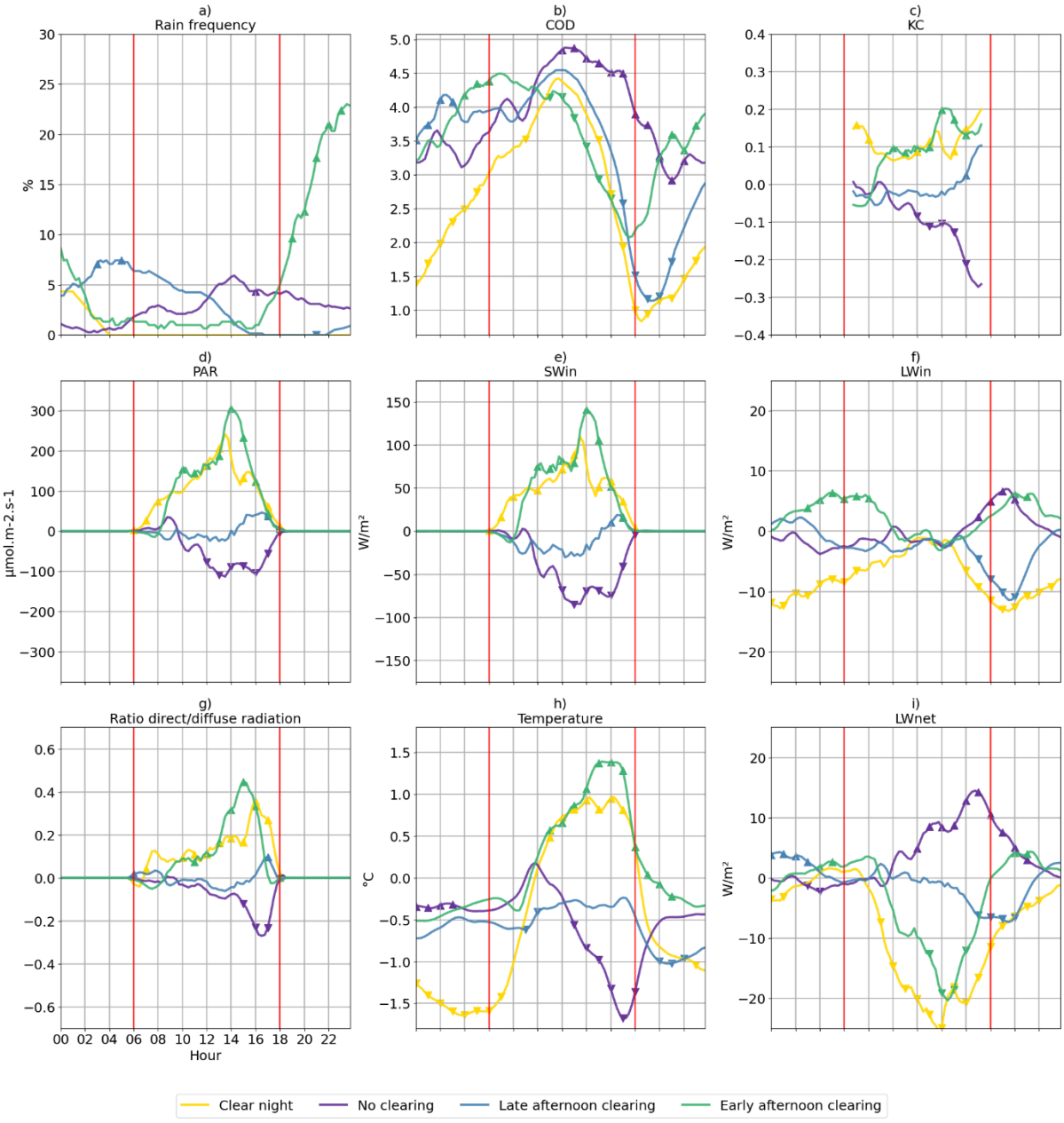

Figure 5: a) 3-h rolling mean of rainfall frequency, b) 1-h rolling mean of COD estimated by the camera, c--i) 1-h rolling mean of deseasonalized anomaly of the meteorological parameters acquired by the weather station. Up pointing triangle: higher values than the 97.5th percentile. Down pointing triangle: lower values than the 2.5th percentile. Red lines: sunrise and sunset. X-axis: Local time.

2) LIGHT AND WATER AVAILABILITY

The quantity of light available for trees photosynthesis as measured with a PAR sensor (in µmol/m².s), and its "quality" as evaluated from the ratio of the direct to diffuse radiation are shown in Figure 5d-g for each type. On EaC and CNi days, the quantity of light available for trees photosynthesis is significantly larger than on LaC and NoC days, up to 400 µmol/m².s

Accepted for publication in *Journal of Applied Meteorology and Climatology*. DOI 10.1175/JAMC-D-23-0225.1.

more on EaC days as compared to NoC days (and 100 μmol/m².s more as compared to CNi). However, the direct component largely dominates the diffuse one with a ratio anomaly around 0.2 (i.e., +20%) on average, and reaching 0.4 (i.e., +40%) on EaC days in the afternoon. Although there is less light available on LaC and NoC days, the photosynthesis can nevertheless be supported by the predominance of the diffuse radiation in the afternoon (ratio anomaly below -0.2) which propagates more through the canopy, reaching more leaves (while direct radiation mainly affects the canopy with saturation effects (Mercado et al. 2009; Liu et al. 2021).

With regards to water availability, rainfall is infrequent during the dry season (Figs 2 and 5a). CNi days are always fully dry. Rainfall is slightly more frequent during LaC and NoC days, but frequencies remain below 10% and their timing is different: in the early morning on LaC days and in the early afternoon on NoC days. The EaC days are the wettest with frequencies above 10% from 20.00 to noon (peaking at 25%). This is not surprising as these days are the most frequent in May and October which are transition months between the dry and the rainy seasons.

In terms of water demand, the range of daily ETo for each type is depicted in Figure 6. ETo anomalies are the highest during the EaC days with a median above +0.5mm/day. Anomalies are also mostly positive on CNi days with a median around +0.25mm/day. This is expected since those types have the highest positive anomalies of incoming shortwave radiation and temperature, two variables important for the computation of ETo. On the opposite, on the NoC days, ETo anomalies are mostly negative (median at -0.5mm/day) but with the largest variance. As for the radiation anomalies, LaC days are associated with the weakest anomalies: the median is -0.2 mm/day.

The larger water demand on the EaC days might be partly compensated by the higher frequency of rainfall. But the moderate demand on CNi days might be more critical for forests functioning as these days are totally dry.

Accepted for publication in *Journal of Applied Meteorology and Climatology.* DOI 10.1175/JAMC-D-23-0225.1.

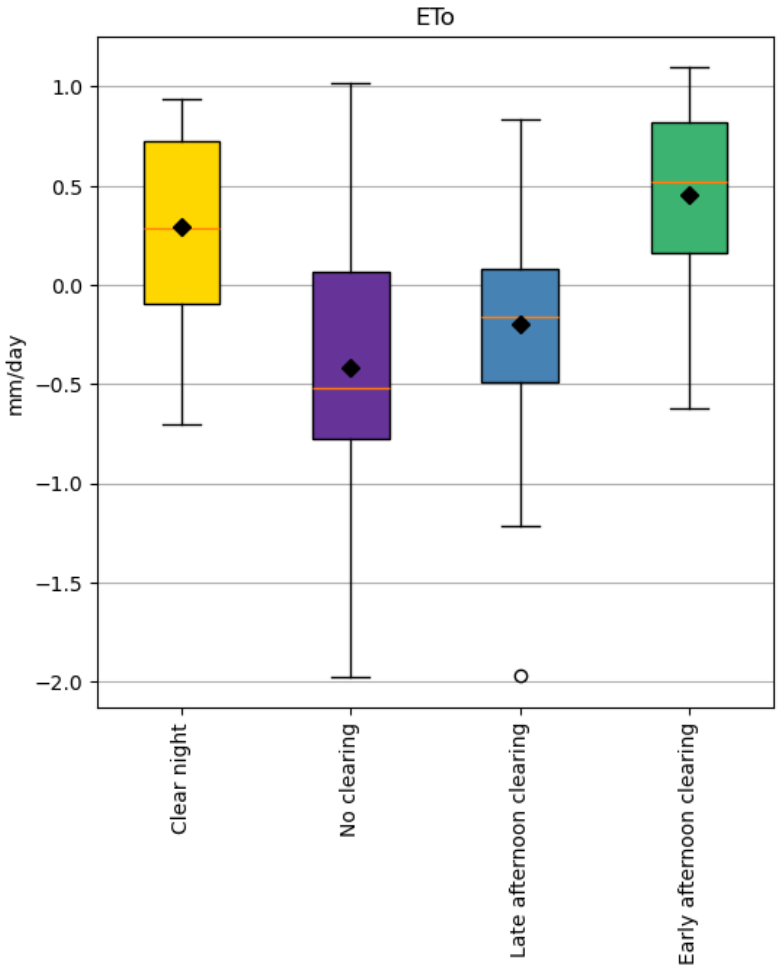

Figure 6: Boxplots of deseasonalized daily ETo anomalies by canonical type. The median of each type is represented with an orange line and the mean with a black diamond.

d. Space-time cloud cover dynamics from SAFNWC cloud products:

As a last step of our study, we complete our analysis of the total cloud cover over Bambidie using satellite estimates of CTYPE and CTH from SAFNWC. The questions we seek to answer are:

Which differences do we observe in the type of clouds in presence between the 4 canonical types? How frequent are low-level clouds? To what extent is the cloud evolution observed with the IR Camera at Bambidie representative of a wider area?

1) CLOUD TYPES AND THEIR DIURNAL EVOLUTION FOR THE 4 TYPES OF DAYS

To begin with, we assess the performance of SAFNWC in estimating the TCF at Bambidie. The comparison between the TCF from the IR camera and the SAFNWC at a daily time-step is shown in Figure 2b. The correlation between these two time-series equals 0.64 (significant

Accepted for publication in *Journal of Applied Meteorology and Climatology.* DOI 10.1175/JAMC-D-23-0225.1.

at the 95% level). Given that the SAFNWC cloud product usually underestimates the low-level cloud cover during the night (Dommo et al. 2018; Champagne et al. 2023), we also computed the correlations between the IR camera and the SAFNWC TCF separately for night-time and daytime. However, we didn't find any significant difference between the two periods (0.55 during the night, 0.57 during the day).

Second, to assess the type of cloud in presence and the way they shape the TCF, Figure 7 shows for each of the 4 types of days, the camera TCF diurnal evolution (black curve and right y-axis upscaled from the 30-seconds to the hourly resolution as compared to Figure 3a) and the corresponding frequency of the 7 CTYPEs retained (cf. section 2.3) from SAFNWC, considering 9 pixels around the station. A direct comparison between the satellite and the camera TCF can be made as the uppermost bars (brown ones) represent the cloud free land, so the upper part of the underlying bars (light blue ones) corresponds to the satellite's TCF. Hours when frequencies are significantly different from chance are shown with white hatches, pointing upwards for frequencies higher than those expected by chance, and downwards for frequencies lower than those expected by chance.

Overall, the diurnal cycles of the satellite and camera TCF match well, with correlations always >0.7 whatever the class. The biases of the satellite TCF (difference between the black curve and the top of light blue bar, Figure 7) are the lowest during daytime especially in mornings (<0.2 from 08.00 to 12.00) while they remain stable during night-time, around 0.25. Except on NoC days, biases switch from negative values (i.e. satellite detects less clouds than the camera) between late night/early morning around sunrise to positive ones in late afternoon/early evening around sunset. The biases are also larger on CNi days during late night when the cloud cover resettles, and on EaC days, during afternoons when the cloud cover disappears (Figure 7). This flip in the bias sign may be partly related to the diurnal cycle of the humidity content. Water-vapor content strongly modulates the amount of IR emission (Shaw and Nugent 2013). In late night/early morning at Bambidie, the air mass is usually saturated in water vapor (mean relative humidity equals 100% at 6 am independent of the diurnal types) and fog is frequent. This can be interpreted as cloud cover by the camera, while such ultra-low clouds are not detected by the satellite. In addition, small droplets of dew, not accurately identified by the camera can also positively distort the cloud cover estimate.

During daytime, low and very low clouds frequency is superior to 30% around noon according to the satellite estimates. Their frequency systematically sharply increases till noon

Accepted for publication in *Journal of Applied Meteorology and Climatology.* DOI 10.1175/JAMC-D-23-0225.1.

and then sharply decreases till sunset. The specificity of the NoC days is mostly explained by the low clouds. These latter are much more frequent in those days (significantly from 13.00 to 00.00), a frequency which keeps increasing to reach 40% until sunset. In the late night, very low clouds are also significantly more frequent, around 8%.

Regarding days with an afternoon clearing, the EaC days differ from the LaC and CNi days with a significantly larger frequency of fractional clouds in the afternoon (~20%) and then, from 19.00 to 00.00, high opaque clouds become significantly predominant (~30%). This suggests first that during EaC days low-level clouds tend to evolve from stratiform towards convective clouds, rather than dissipating. This also explains the higher frequency of rains by night on EaC days (Figure 5a). Second, it also suggests positive feedback with SW incoming radiation which depicts the highest anomalies (Figure 5e): as the cloud cover breaks-up, more energy is received at the surface which favors in turn the cloud cover dissipation.

On LaC days, it should be noted that the opaque clouds are significantly more frequent around sunrise, which is consistent with higher rain frequency at that time as compared to the rest of the day (Figure 5a). Lastly, on CNi days, as expected, cloud free land frequency is significantly higher from 00.00 to 09.00. But these days are also characterized by a significantly larger frequency of very low clouds in late morning (>40%).

Accepted for publication in *Journal of Applied Meteorology and Climatology.* DOI 10.1175/JAMC-D-23-0225.1.

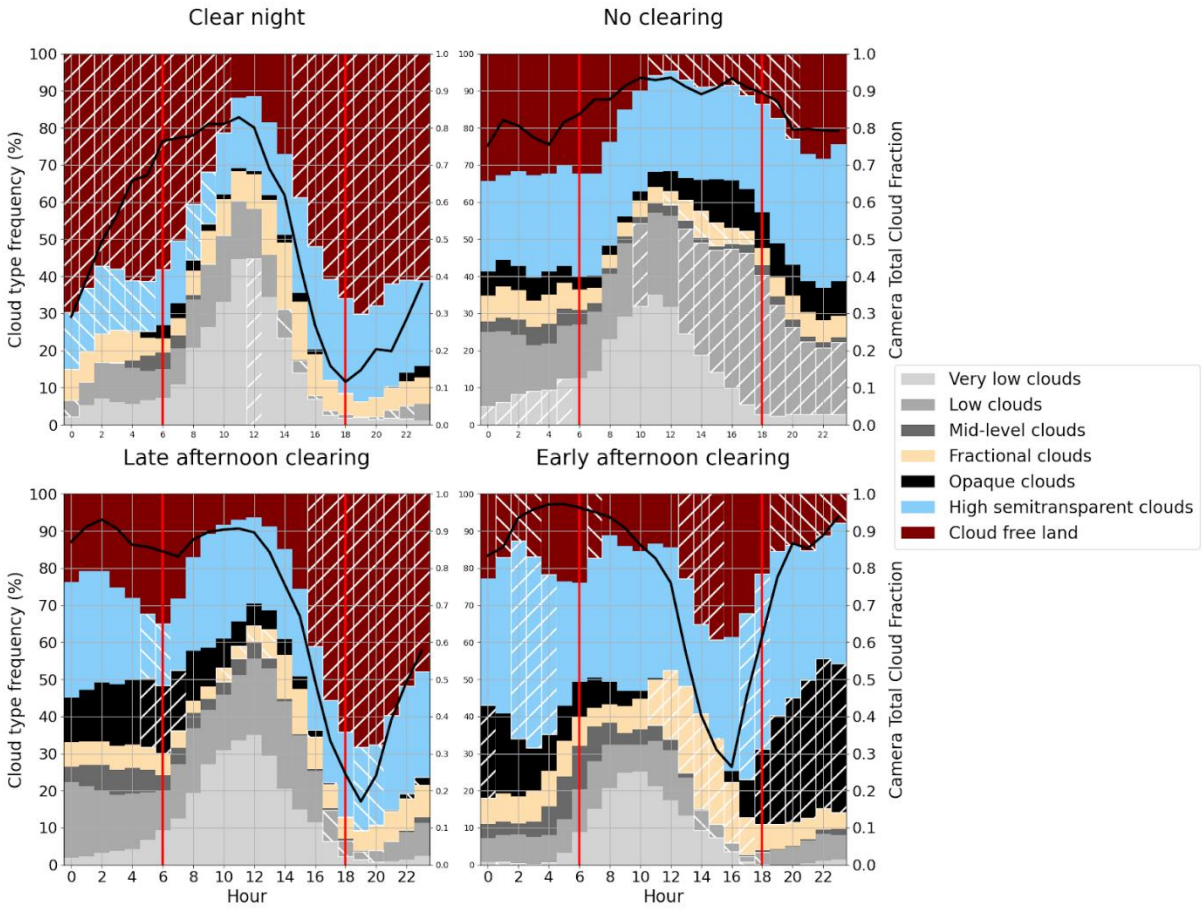

Figure 7: Bars: 2-hour rolling mean of frequency of occurrence of the 7 CTYPEs (from SAFNWC) along the diurnal cycle for the four canonical types considering 9 pixels around Bambidie. Black line: the corresponding diurnal cycle of IR camera TCF. Red lines: sunrise and sunset. Upward pointing white hatches: values greater than the 97.5th percentile; downward pointing: values lower than the 2.5th percentile. X-axis: Local time.

One of our hypotheses is that on some days the clearings in the total cloud cover come from the evolution of the stratiform low-level clouds towards a more convective and fractionated cloud cover i.e., from stratocumulus towards cumulus and later towards cumulonimbus if conditions are met for deep convection to be triggered. This diurnal evolution has been suggested using low-level cloud data from a larger set of ground observations (Moron et al. 2023) or the European Reanalysis (Dommo et al. 2022). This should be especially true at the beginning and end of the dry season at Bambidie.

To further document such an evolution, we assessed the changes in terms of cloud top altitude using the SAFNWC Cloud Top Temperature and Height product. Figure 8 presents the evolution of the cloud top height (CTH) anomaly along the diurnal cycle for each canonical type.

Accepted for publication in *Journal of Applied Meteorology and Climatology*. DOI 10.1175/JAMC-D-23-0225.1.

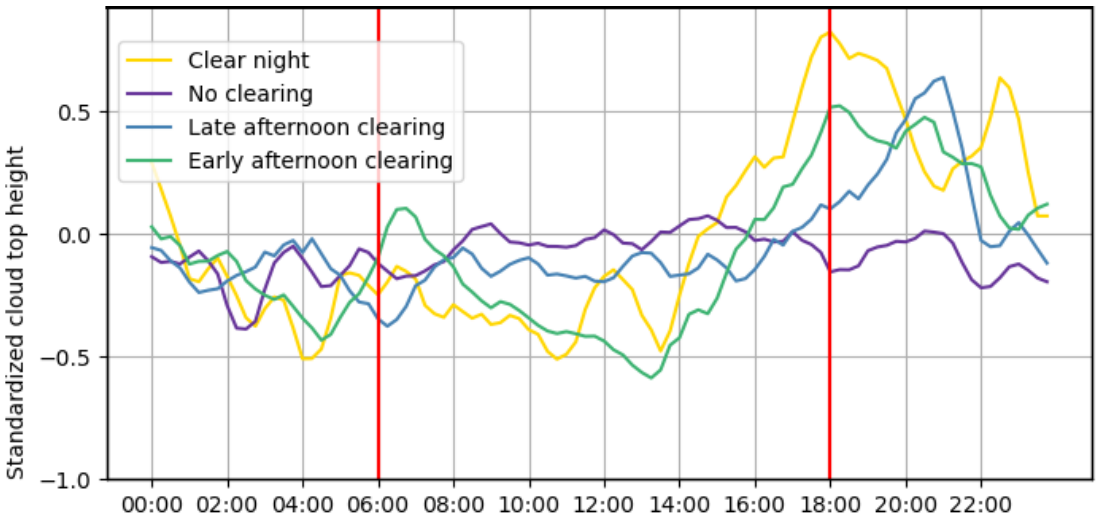

Figure 8: 1-h Rolling mean of standardized CTH along the diurnal cycle for the four canonical types and considering 9 pixels around Bambidie. X-axis: Local time.

In the late night, there are few differences in CTH between the four types, as the differences appear after 08.00. Until 14.00, CTH is almost always negative for all the types: clouds tend to have a lower CTH than normal. This is especially so for the CNi and EaC days suggesting a lower morning cloud cover during these days and is concordant with the fact that, on CNi days, very low clouds are significantly more frequent in late morning (Figure 7). As expected, CTH anomalies on the NoC days depict very few changes which illustrate the temporal stability of the cloud cover and the low-level cloud deck, along the whole day.

On Eac and CNi days, CTH anomalies increase to become positive (and >0.5 std) from 14.00 until noon while on LaC days, CTH anomalies increase later, from 16.00. For these three types, these increases suggest a change in the cloud cover properties, from stratiform to cumuliform, in agreement with changes in the types of clouds noticed in Figure 7. It should be also noted a time lag of about 2 hours between the lowest TCF and highest CTH for LaC and EaC days. The fragmentation or dissipation of the stratiform cloud deck is firstly recorded in the decrease of the TCF, but the CTYPE also changes, from stratiform to convective clouds (Moron et al. 2023), thus the increase of CTH.

2) Spatial representativeness of cloud cover evolution at Bambidie

A final important question is that of the spatial representativeness of the TCF diurnal evolutions observed at Bambidie during the 2022 dry season. Are these diurnal evolutions purely local or do they concern a wider area? This would suggest that the atmospheric dynamics processes involved, especially those leading to the cloud cover clearing, are of large scale. To

Accepted for publication in *Journal of Applied Meteorology and Climatology*. DOI 10.1175/JAMC-D-23-0225.1.

address this question of the spatial representativeness, we again use SAFNWC retrievals extracted over the area 4.25°S-3.25°N / 7.5-16.5°E documenting most of Western Central Africa.

First, TCF estimated from SAFNWC for the pixel of Bambidie at 15-min resolution is correlated with that of all the pixels in the entire sub-region (Figure 9). This allows us to assess the "speed" of the spatial decorrelation of cloudiness variations. As expected, the highest correlations (>0.4) are observed in the vicinity of Bambidie, then in the east part of Gabon. The Chaillu mountains, to the west, show a rapid decrease in the correlation values, suggesting a different cloud cover dynamics over the coastal plains, and the windward slopes of the mountains. On the other hand, the Cristal mountains to the north and the Batéké plateaux to the south-east are not associated with such rapid spatial decorrelation.

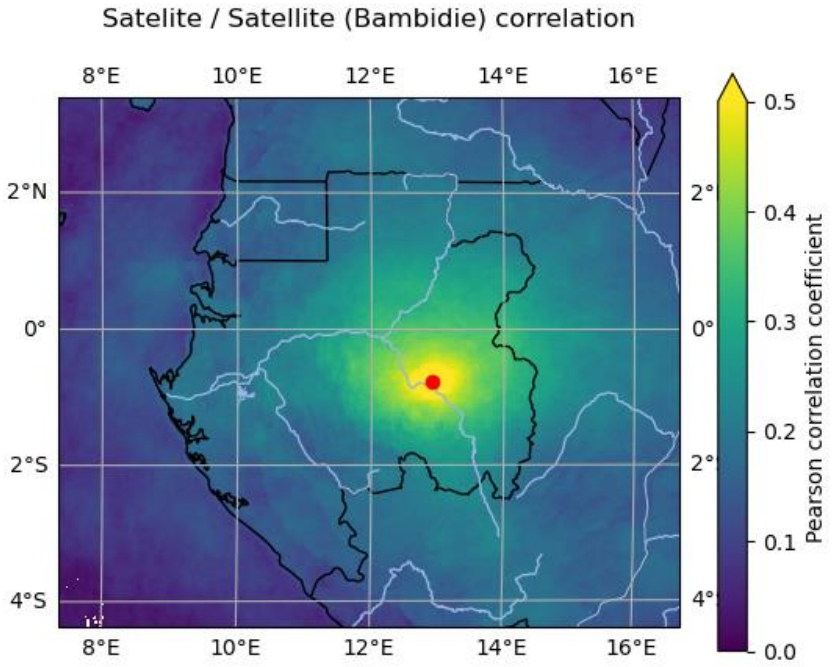

Figure 9: Spatial Pearson correlation coefficient between satellite TCF and satellite TCF at Bambidie (15-min resolution, red dot). White dots correspond to pixels with non-significant correlation (p_value<0.05).

Second, we built-up composite fields of frequency anomalies for the low cloud cover (Figure 10) by grouping the very low and low clouds frequencies, in order to assess their spatial dynamics along the diurnal cycle (every two hours) for the 4 types. We focus on the low cloud cover because very low and low clouds are predominant in the total cloud cover (Figure 7). Results for the TCF are shown in supplementary materials (Figure S4).

Accepted for publication in *Journal of Applied Meteorology and Climatology.* DOI 10.1175/JAMC-D-23-0225.1.

Looking at Figure 10, it is striking to see that, except for LaC days (panel c, for which there is no significant signal apart from negative anomalies East of Bambidie at 18:00), the diurnal evolution of the low-level cloud cover at Bambidie is not strictly local but part of an evolution at a wider spatial scale.

Regarding CNi days (Figure 10a), a significant increase of the low-level cloud cover in the morning also affects the Mont de Cristal area in the northwest of Gabon. The afternoon clearing observed at the station, sets-up first in the Republic of Congo and the plateaux Batéké, then propagates along the Oogoué valley until 20.00. Then it weakens but remains significant in the vicinity of Bambidie until midnight. The dissipation signal is much stronger in the TCF (Figure S4): the negative anomalies are large and widespread indicating that most CTYPEs, and not just the low ones, are globally less frequent over the region.

On NoC days, the abnormally high frequencies of low clouds during the afternoon and the early night at Bambidie (Figure 7) concern half of the Gabon (Figure 10b), but the anomalies first confined to the southeast of Gabon in the afternoon, then propagate through the Oogoué valley, and spread westward in the early night. The TCF composites (Figure S4) also show that more clouds are detected at the border with the Republic of Congo and Cameroon, suggesting that during NoC days, the cloud cover extends further east than normal.

The EaC days are the ones displaying the lowest day-time frequencies of very low and low clouds with the earliest dissipation (from 10.00, Figure 7). Such a quick and early dissipation of the low-cloud deck is of very large scale (Figure 10d) as the negative anomalies concern most of Gabon. At 12.00, half of Gabon is affected by this dissipation of low clouds. Then anomalies strengthen until 16.00 and propagate westwards beyond the Chaillu mountains but without reaching the coast to the south, being blocked by the Mayombé mountains. From 20.00 anomalies are losing their spatial coherence but are still marked on the windward slopes of the Chaillu and Cristal mountains. However as suggested by the TCF composites (Figure S4), the cloud cover resettles quickly in the evening (with opaque clouds Figure 7), a signal coming from the south-east.

Lastly, on LaC days (Figure 10c) there are no significant anomalies except for negative ones around Bambidie at 18:00. The lack of significance implies that the low-level cloud cover diurnal evolution on these days is typical of a dry season over the whole Gabon, but that the clearing of low clouds at 18.00 is more pronounced around Bambidie.

Accepted for publication in *Journal of Applied Meteorology and Climatology.* DOI 10.1175/JAMC-D-23-0225.1.

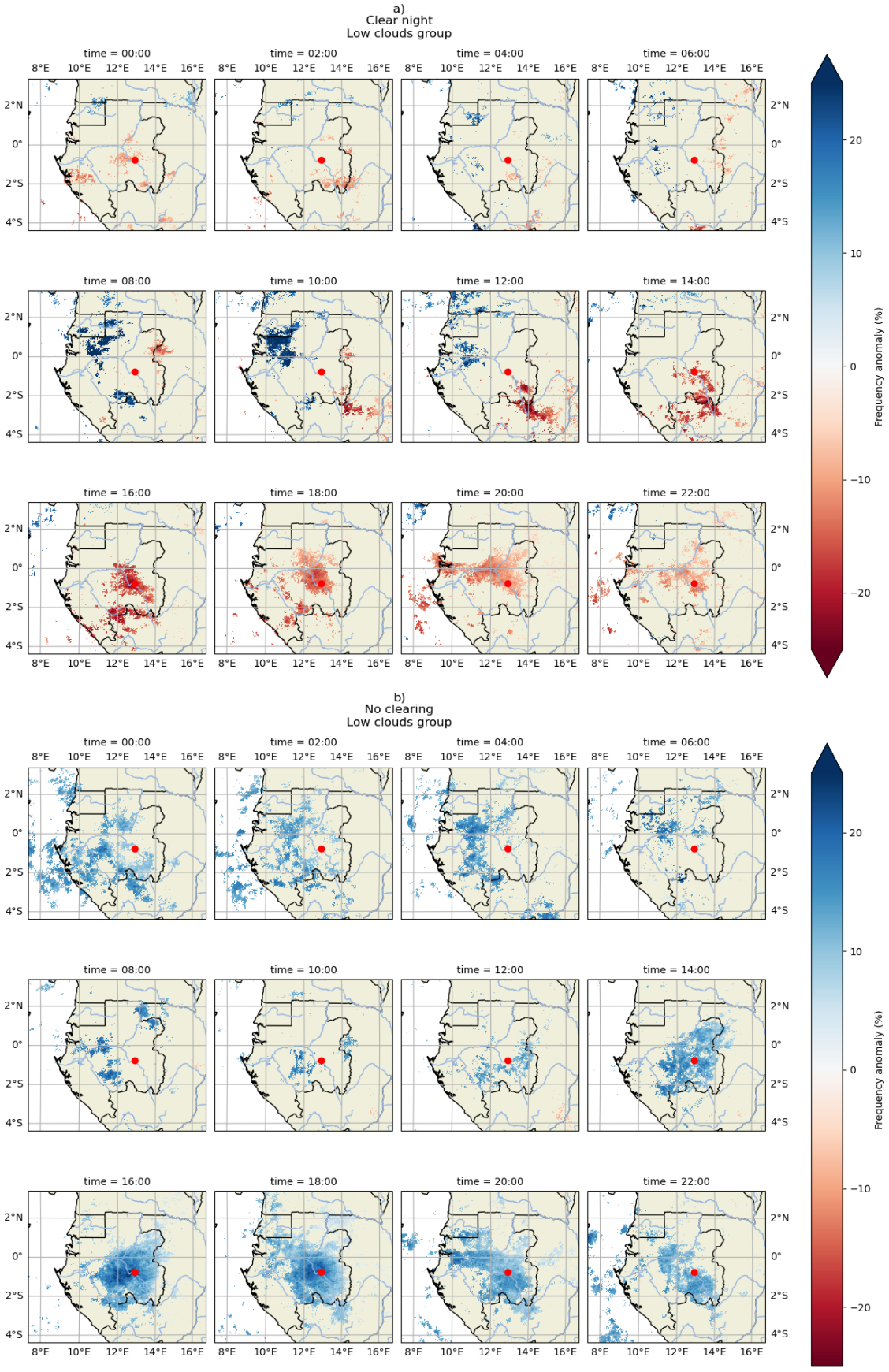

Accepted for publication in *Journal of Applied Meteorology and Climatology*. DOI 10.1175/JAMC-D-23-0225.1.

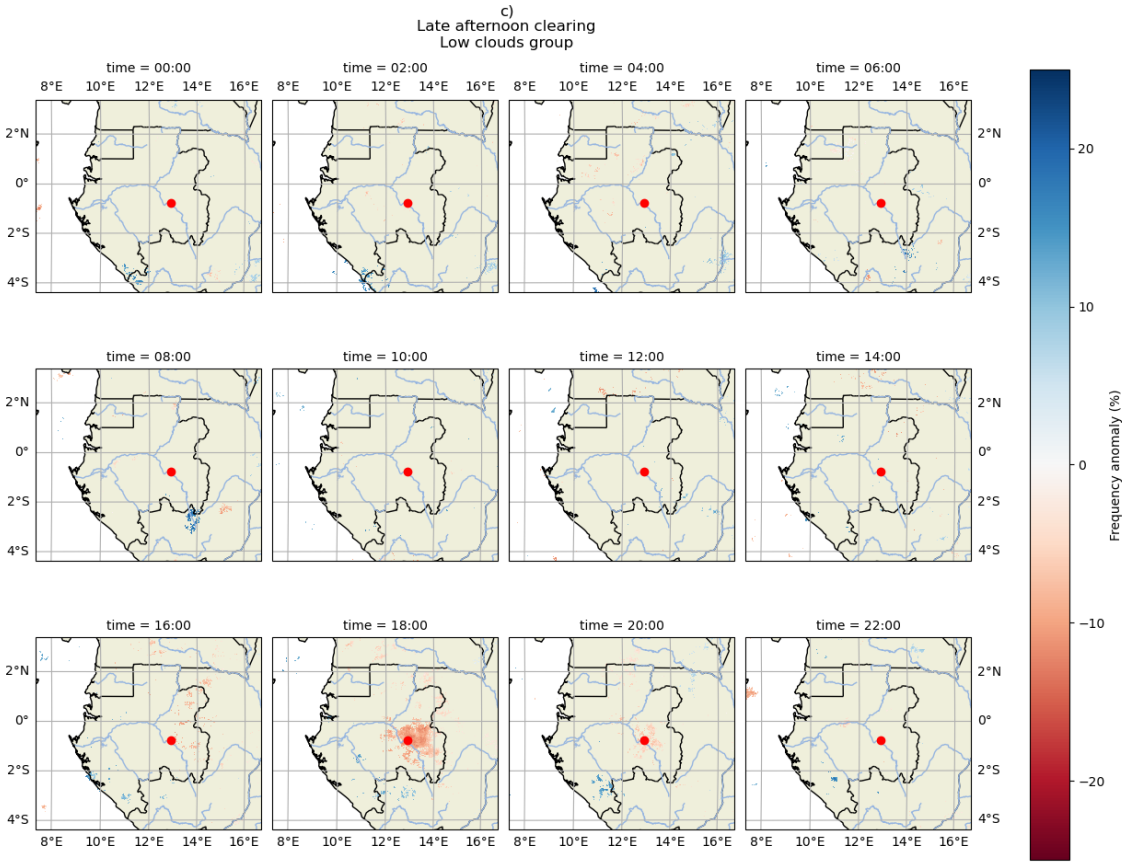

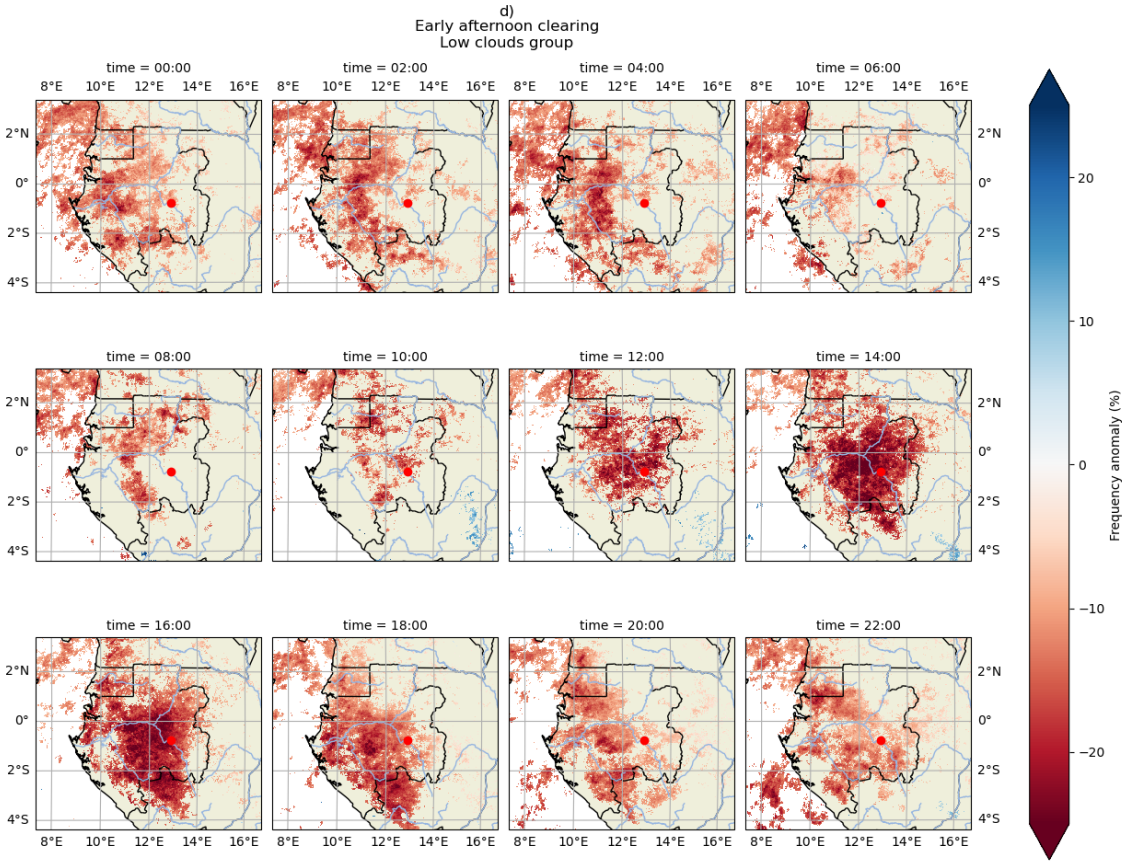

Accepted for publication in *Journal of Applied Meteorology and Climatology*. DOI 10.1175/JAMC-D-23-0225.1.

Figure 10: Low clouds (very low and low) frequency anomaly for: a) “clear night”, b) “no clearing”, c) “late afternoon clearing”, d) “early afternoon clearing” types. Only the significant anomalies are shown. Hours are in local time. The red dot denotes Bambidie.

The above analyses confirm that the diurnal evolutions of the TCF observed at Bambidie are part of large-scale changes in the cloud cover over WCA, especially the low-level cloud cover. However, they do not provide information on the synchronism of the 4 typical diurnal evolutions extracted at Bambidie in the region as a whole. In other words, what is the probability of observing one of the 4 canonical types in any part of the region when a given type is observed in Bambidie?

To address this point and as a last step of our study, the IR camera classification is first projected onto the satellite TCF for Bambidie’s pixel. Then the 4 types obtained from the satellite TCF at Bambidie are used to classify the satellite TCF for each day and each pixel of WCA using the minimal Euclidean distance. This “indirect” approach allows us to take partly into account the biases of TCF in the satellite. Then, from this new classification, we computed the frequency of occurrence of each of the 4 types at each pixel given the diurnal evolution recorded at Bambidie with the IR camera, i.e., the “conditional” probability. Results are plotted in Figure 11 as maps of the most frequent class encountered at each pixel of WCA for each of the 4 types observed at Bambidie with the IR camera. The corresponding frequency values are shown in Figure S5.

Overall, and in line with the above maps of anomalies in the frequency of low clouds (Figure 10), for most of the 4 types of days observed at Bambidie, the spatial coherency is quite strong over WCA. On NoC days at Bambidie (Figure 11 top right panel), i.e., when the cloud cover does not clear in the afternoon, the probability of observing a NoC day over the whole Gabon, Equatorial Guinea and South and Center Republic of Congo is high (above 50% over the Western and central parts of Gabon, Figure S5). It is the same on EaC days (Figure 11, bottom right panel) which are highly probable (above 50%) over the eastern part of Gabon when EaC days are recorded at Bambidie, while at the coastal fringe, the NoC days are the most probable. The spatial pattern associated with LaC days at Bambidie (Figure 11 bottom left panel) is characterized by an East-West gradient: the cloud cover dissipates in the early afternoon over the plateaux to the East (EaC days are the most probable), in the late afternoon at Bambidie and over the whole area to the lee of Mont Chaillu, while it does not dissipates at all to the West on the windward slopes (NoC days are the most probable). Lastly, on CNi days at Bambidie, the spatial coherence is the weakest. Nights also tend to be clearer to the lee of

Accepted for publication in *Journal of Applied Meteorology and Climatology.* DOI 10.1175/JAMC-D-23-0225.1.

Mont Chaillu, over the coastal fringe and the South of the Republic of Congo, but on the windward slopes of Mont Chaillu, days are cloudier, either of the NoC or LaC type. Note that as compared to NoC and EaC days, the frequency values (Figure S5) for LaC and CNi days are lower, confirming a weaker spatial coherence of the diurnal evolution of the TCF across WCA during these later types of days.

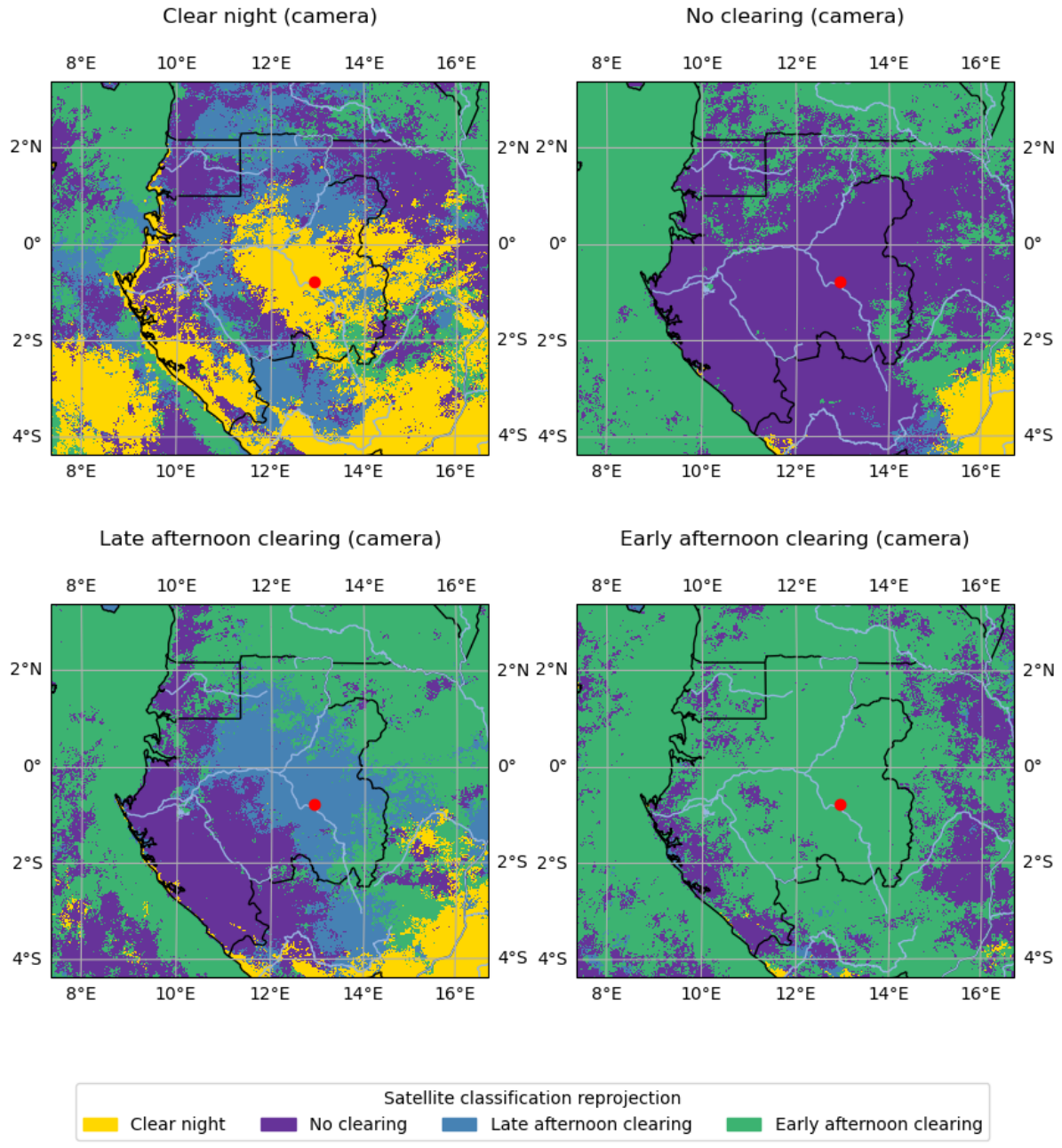

Figure 11: Most frequent type observed at each pixel of the study area (according to the K-means centroids projection onto the satellite TCF) given the type observed with the IR camera at Bambidie (red dot).

4. Discussion and conclusion

Accepted for publication in *Journal of Applied Meteorology and Climatology*. DOI 10.1175/JAMC-D-23-0225.1.

The aim of this study was twofold: (1) to gain a better understanding of the diurnal evolution and spatial scale of the low-level cloud cover variations during the dry season in Western Central Africa and, (2) to assess its impacts on the energy budget, water demand and light availability for forests functioning. The analysis started from high resolution (30 seconds) TCF and COD records from an IR camera located at Bambidie, in eastern Gabon, from May to October 2022. As this season is mostly dry with a high mean TCF (~0.75), TCF values should be usually interpreted as low-level cloud cover fraction, except in May or September, when scattered rain occurs sometimes and when TCF may represent a mixture of low stratiform and convective cloud bases. TCF and COD were cross-analyzed with records from a weather station (radiation, temperature, rainfall, etc.) installed in March 2020 and with cloud products (cloud fraction, CTYPE and CTH) supplied by SAFNWC, and derived from measurements by MeteoSat Second Generation. These cloud products were used to document cloudiness characteristics (e.g. the type of cloud present) and assess the spatial representativeness of observations made locally with the IR camera.

First, the TCF diurnal variations were reduced to 4 canonical types using a K-means classification. The 4 types are mostly defined by the TCF variability in the afternoon and early night. This diurnal evolution fits well with the one depicted in previous studies using a larger space-time, but low resolution, sample than here (Dommo et al. 2018; Champagne et al. 2023; Moron et al. 2023). However, it is slightly different from the one observed in Southern West Africa during the same calendar season. There, the low-level cloud cover deck usually establishes around midnight, lasts between 2h and 9h, and therefore fully dissipates before midday (Adler et al. 2019; van der Linden et al. 2015; Lohou et al. 2020). Amongst the 4 types extracted, three show substantial afternoon clearings with different starts and lengths ("clear night" with TCF < 0.5 between 15.00 and 00.00, "late afternoon clearing" from 16.30 to 22.30, "early afternoon clearing" from 14.00 to 17.30) while one does not show any clearing ("no clearing"). Overall, the "no clearing" (37%) and the "late afternoon clearing" days (31%) are the most frequent and are predominant during the heart of the dry season (July-August). The "clear night" and "early afternoon clearing" days are less frequent (respectively 13% and 18 %) and mostly observed in May and September.

As the TCF in WCA during the dry season is mainly composed of low-level clouds, our classification can be compared with the one by Moron et al. (2023). In their study, these authors used a dataset of ground observations of low-level clouds for 26 synoptic stations over Gabon,

Accepted for publication in *Journal of Applied Meteorology and Climatology*. DOI 10.1175/JAMC-D-23-0225.1.

southern Cameroon and Republic of Congo in May-October 1971-2019. They extracted 3 canonical types of low-level cloud fraction: a clear type with a low-level cloud fraction roughly lower than 2 oktas all day long, a clear afternoon type and a dark type with overcast conditions all day long. These last two types are similar to our "early afternoon clearing" and "no clearing" classes while their first type is not found with the IR camera classification. These differences can be easily explained by the fact that (i) we consider the total and not the low-level cloud fraction only; (ii) our temporal sampling is limited to only one dry season; (iii) our spatial sampling of only one station, located in the transition between the cloudiest zone to the west and the least cloudy in the east (Champagne et al. 2023; Moron et al. 2023) prevents the detection of any clear diurnal type.

Then, a composite analysis of the COD and the meteorological parameters from the weather station was performed to assess the differences between the 4 canonical types in terms of energy budget (net, incoming and outgoing SW and LW radiation), light availability (PAR and ratio of the direct and diffuse radiation) and water demand (evapotranspiration). The COD diurnal evolutions merely mirror those of TCF as the cloud cover is dominated by low-level clouds: as they break-up and thin (set-up and thick) their optical depth decreases (increases).

Logically the "No Clearing" type is characterized by the strongest deficit in net radiation due to a 50W/m2 deficit in incoming SW radiation which cannot be offset by the weak excess (10W/m2) in net LW radiation. Although light availability (PAR) is the lowest on these days (-100μmol/m².s), the diffuse radiation dominates (+20%), which is thought to favor photosynthesis within the canopy (Mercado et al. 2009; Liu et al. 2021). These days are also the ones with the lowest water demand (-0.3mm/day), so minimizing the water stress.

On the other hand, the "Clear Night" type combines a moderate excess of net radiation (due to a large excess of incoming SW and a weak deficit in LW radiation) and of light available for photosynthesis (+100 μmol/m².s), mainly in the form of direct radiation (+20%). They record a higher water demand (+0.6mm/day) and are fully dry therefore more "Clear Night" days, especially towards the heart/end of the dry season (i.e., when the soil water content has been greatly depleted) may be detrimental for the forests.

The "Early afternoon Clearing" type is the one with the largest surplus of incoming shortwave radiation mainly in the form of direct radiation (+40%), and PAR (+400 μmol/m².s). LW incoming radiation is also the highest at sunrise and after sunset, as the cloud cover is then even more important than on "No Clearing" days. These days, the warmest on average, are

Accepted for publication in *Journal of Applied Meteorology and Climatology*. DOI 10.1175/JAMC-D-23-0225.1.

characterized by the highest water demand (+0.5mm/day), but rainfall can occur from time to time mostly in the early night.

Lastly, the “Late afternoon Clearing” days are the closest to the seasonal average day as deviations from the mean are most of the time not significant for most of the meteorological parameters analyzed.

Satellite imagery provides additional insights to the measurements with the IR camera. The SAFNWC CTYPE product confirms that the TCF at Bambidie is mainly composed of low and very low clouds which agrees with studies by Moron et al. (2023) and Champagne et al. (2023). The low and very low clouds frequency usually increases until noon then decreases till sunset on “Clear Night", “Early” and “Late afternoon Clearing” days while it remains important on the “No Clearing” type. As the low-level clouds frequency decreases, the fractional clouds frequency increases, especially on “Early afternoon Clearing” days. On these later days, the frequency of high opaque clouds is significantly higher during the first part of the night which is in line with the higher frequency of rainfall recorded at that time by the weather station.

Therefore, on some days, the clearings in the total cloud cover seem to come from the evolution of the stratiform low-level clouds towards a more fractionated and possibly convective cloud cover: i.e., from stratocumulus towards cumulus and later towards cumulonimbus if conditions are met for deep convection to be triggered. This diurnal evolution has been also proposed in the study by Champagne et al (2023). Similarly, in Southern West Africa, Dione et al. (2019) and Lohou et al. (2020) showed that the break-up of the stratus deck is associated with an increase of its base height indicating an evolution towards a convective phase, especially convective shallow cumulus. This could be also interpreted as positive feedback of the increase in incoming SW radiation due to cloud cover fractioning.

Satellite clouds products also enabled us to assess whether these canonical types are of local-scale only or of a larger spatial scale. It appears that the signal recorded with the IR camera at Bambidie is usually not purely local. For example, most of Gabon and Southwestern Republic of Congo experiences NoC or EaC days when these types of day are observed at Bambidie. Interestingly, on days with a late break-up of the low-clouds cover (LaC days) at Bambidie, the western part of Gabon and Southwestern Republic of Congo tend to experience little clearing (the NoC days are there the most frequent), while in the eastern Gabon, the break-up tends to be earlier (the EaC days are the most frequent). These findings thus confirm and refine studies by Dommo et al. (2018) and Moron et al. (2023) which suggest that there are

Accepted for publication in *Journal of Applied Meteorology and Climatology.* DOI 10.1175/JAMC-D-23-0225.1.

differences in the low-level cloud cover diurnal evolution between the eastern and western parts of Gabon and Southwestern Republic of Congo. These zonal differences may be triggered by the interaction between the usual low-level southwestern winds, advecting cool and relatively moist air from the equatorial Atlantic (Dommo et al. 2018; Moron et al. 2023) and the topography, especially the Massif de Chaillu. The separation between the zones where the "no clearing" and the "afternoon clearing" types dominate, matches well with the separation between the windward and downward slopes of this low-altitude mountain. A modest leeward foehn effect is hypothesized to be instrumental to enhance the afternoon clearings, then the increasing incoming solar radiation at the surface due to fragmentation of the stratiform cloud deck may warm the surface and low level atmosphere thus possibly triggering more or less intense convection.

The questions left open are (i) the thermodynamic processes behind these different diurnal evolutions: they are still unknown for the region and deserve being studied but would require dedicated field measurements such as those developed in Southern West Africa by Lohou et al. (2019) and (ii) the interannual variability and long term evolution of the 4 canonical types obtained: as the satellite TCF is well correlated with the IR camera TCF, the classification could be extended to the whole period covered by the satellite estimates and the whole Western Central Africa.

Acknowledgments.

This study is part of the project "Dynamics, Variability and Bioclimatic Effects of Low Clouds in Western Central Africa" (DYVALOCCA, https://dyvalocca.osug.fr/) funded by the French Agence Nationale de la Recherche (ANR) and the German Deutsche Forschungsgemeinschaft (DFG) from January 2020 to June 2023 under contract ANR- 19-CE01-0021 and DFG FI 786/5-1, respectively, and by the Centre National d'Etudes Spatiales (CNES TOSCA). It contributes also to the International Joint Laboratory "Dynamics of land ecosystems in Central Africa in a context of global changes" of the Institut de Recherche pour le Développement (LMI DYCOFAC IRD, https://www.lmi-dycofac.org/). Computations were performed using HPC resources from DNUM CCUB (Centre de Calcul de l'Université de Bourgogne), Dijon, France. The authors would like to thank Precious Woods - CEB (preciouswoods.com, committed to certified and sustainable management of tropical forests) for hosting their field measurements from March 2020 to March 2023 in Bambidie, and the ICARE data center (icare.univ-lille.fr) for its support regarding the SAFNWC cloud products.

Accepted for publication in *Journal of Applied Meteorology and Climatology.* DOI 10.1175/JAMC-D-23-0225.1.

Data Availability Statement.

SAFNWC cloud products on MSG-0 imagery are available on the ICARE website (https://www.icare.univ-lille.fr/asd-content/extract/subset/ordergeo). The camera and weather station data will be made available on the website https://www.easydata.earth.

REFERENCES

Adler, B., K. Babić, N. Kalthoff, F. Lohou, M. Lothon, C. Dione, X. Pedruzo-Bagazgoitia, and H. Andersen, 2019: Nocturnal low-level clouds in the atmospheric boundary layer over southern West Africa: an observation-based analysis of conditions and processes. *Atmospheric Chemistry and Physics*, **19**, 663–681, https://doi.org/10.5194/acp-19-663-2019.

Aellig, R., V. Moron, P. Camberlin, O. Champagne, N. Philippon, A. H. Fink, and P. Knippertz, 2022: Cloud observing data of 85 stations in western Central Africa. https://doi.org/10.5445/IR/1000150635.

Berry, Z. C., and G. R. Goldsmith, 2020: Diffuse light and wetting differentially affect tropical tree leaf photosynthesis. *New Phytologist*, **225**, 143–153, https://doi.org/10.1111/nph.16121.

Bertin, C., S. Cros, L. Saint-Antonin, and N. Schmutz, 2015: Prediction of optical communication link availability: real-time observation of cloud patterns using a ground-based thermal infrared camera. *Optics in Atmospheric Propagation and Adaptive Systems XVIII*, Vol. 9641 of, Optics in Atmospheric Propagation and Adaptive Systems XVIII, SPIE, 66–73.

Champagne, O., and Coauthors, 2023: Climatology of Low-Level Clouds over Western Equatorial Africa Based on Ground Observations and Satellites. *Journal of Climate*, **36**, 4289–4306, https://doi.org/10.1175/JCLI-D-22-0364.1.

Derrien, M., and H. Le Gléau, 2005: MSG/SEVIRI cloud mask and type from SAFNWC. *International Journal of Remote Sensing*, **26**, 4707–4732, https://doi.org/10.1080/01431160500166128.

Derrien, M., and H. Le Gléau, 2010: Improvement of cloud detection near sunrise and sunset by temporal-differencing and region-growing techniques with real-time SEVIRI. *International Journal of Remote Sensing*, **31**, 1765–1780, https://doi.org/10.1080/01431160902926632.

Accepted for publication in *Journal of Applied Meteorology and Climatology*. DOI 10.1175/JAMC-D-23-0225.1.

Dione, C., and Coauthors, 2019: Low-level stratiform clouds and dynamical features observed within the southern West African monsoon. *Atmospheric Chemistry and Physics*, **19**, 8979–8997, https://doi.org/10.5194/acp-19-8979-2019.

Dommo, A., N. Philippon, D. A. Vondou, G. Sèze, and R. Eastman, 2018: The June–September Low Cloud Cover in Western Central Africa: Mean Spatial Distribution and Diurnal Evolution, and Associated Atmospheric Dynamics. *Journal of Climate*, **31**, 9585–9603, https://doi.org/10.1175/JCLI-D-17-0082.1.

Dommo, A., D. A. Vondou, N. Philippon, R. Eastman, V. Moron, and N. Aloysius, 2022: The ERA5's diurnal cycle of low-level clouds over Western Central Africa during June–September: Dynamic and thermodynamic processes. *Atmospheric Research*, **280**, 106426, https://doi.org/10.1016/j.atmosres.2022.106426.

Duveiller, G., P. Defourny, B. Desclée, and P. Mayaux, 2008: Deforestation in Central Africa: Estimates at regional, national and landscape levels by advanced processing of systematically-distributed Landsat extracts. *Remote Sensing of Environment*, **112**, 1969–1981, https://doi.org/10.1016/j.rse.2007.07.026.

Hubau, W., and Coauthors, 2020: Asynchronous carbon sink saturation in African and Amazonian tropical forests. *Nature*, **579**, 80–87, https://doi.org/10.1038/s41586-020-2035-0.

Jedlovec, G. J., S. L. Haines, and F. J. LaFontaine, 2008: Spatial and Temporal Varying Thresholds for Cloud Detection in GOES Imagery. *IEEE Transactions on Geoscience and Remote Sensing*, **46**, 1705–1717, https://doi.org/10.1109/TGRS.2008.916208.

Liandrat, O., S. Cros, A. Braun, L. Saint-Antonin, J. Decroix, and N. Schmutz, 2017: Cloud cover forecast from a ground-based all sky infrared thermal camera. *Remote Sensing of Clouds and the Atmosphere XXII*, Vol. 10424 of, Remote Sensing of Clouds and the Atmosphere XXII, SPIE, 19–31.

van der Linden, R., A. H. Fink, and R. Redl, 2015: Satellite-based climatology of low-level continental clouds in southern West Africa during the summer monsoon season. *Journal of Geophysical Research: Atmospheres*, **120**, 1186–1201, https://doi.org/10.1002/2014JD022614.

Liu, Q., Z. Zhang, M. Fan, and Q. Wang, 2021: The Divergent Estimates of Diffuse Radiation Effects on Gross Primary Production of Forest Ecosystems Using Light-Use

Accepted for publication in *Journal of Applied Meteorology and Climatology*. DOI 10.1175/JAMC-D-23-0225.1.

Efficiency Models. *Geophysical Research Letters*, **48**, e2021GL093864, https://doi.org/10.1029/2021GL093864.

Lohou, F., N. Kalthoff, B. Adler, K. Babić, C. Dione, M. Lothon, X. Pedruzo-Bagazgoitia, and M. Zouzoua, 2020: Conceptual model of diurnal cycle of low-level stratiform clouds over southern West Africa. *Atmospheric Chemistry and Physics*, **20**, 2263–2275, https://doi.org/10.5194/acp-20-2263-2020.

Mercado, L. M., N. Bellouin, S. Sitch, O. Boucher, C. Huntingford, M. Wild, and P. M. Cox, 2009: Impact of changes in diffuse radiation on the global land carbon sink. *Nature*, **458**, 1014–1017, https://doi.org/10.1038/nature07949.

Moron, V., P. Camberlin, R. Aellig, O. Champagne, A. H. Fink, P. Knippertz, and N. Philippon, 2023: Diurnal to interannual variability of low-level cloud cover over western equatorial Africa in May–October. *International Journal of Climatology*, **43**, 6038–6064, https://doi.org/10.1002/joc.8188.

Nam, C., S. Bony, J.-L. Dufresne, and H. Chepfer, 2012: The 'too few, too bright' tropical low-cloud problem in CMIP5 models. *Geophysical Research Letters*, **39**, https://doi.org/10.1029/2012GL053421.

Philippon, N., and Coauthors, 2019: The light-deficient climates of western Central African evergreen forests. *Environ. Res. Lett.*, **14**, 034007, https://doi.org/10.1088/1748-9326/aaf5d8.

Réjou-Méchain, M., and Coauthors, 2021: Unveiling African rainforest composition and vulnerability to global change. *Nature*, **593**, 90–94, https://doi.org/10.1038/s41586-021-03483-6.

Shaw, J. A., and P. W. Nugent, 2013: Physics principles in radiometric infrared imaging of clouds in the atmosphere. *Eur. J. Phys.*, **34**, S111–S121, https://doi.org/10.1088/0143-0807/34/6/S111.

Spracklen, D. V., S. R. Arnold, and C. M. Taylor, 2012: Observations of increased tropical rainfall preceded by air passage over forests. *Nature*, **489**, 282–285, https://doi.org/10.1038/nature11390.

Accepted for publication in *Journal of Applied Meteorology and Climatology*. DOI 10.1175/JAMC-D-23-0225.1.

Wang, Y., and Coauthors, 2021: Day and Night Clouds Detection Using a Thermal-Infrared All-Sky-View Camera. *Remote Sensing*, **13**, 1852, https://doi.org/10.3390/rs13091852.

Accepted for publication in *Journal of Applied Meteorology and Climatology.* DOI 10.1175/JAMC-D-23-0225.1.